PHYSICAL REVIEW B, VOLUME 65, 020407(R)

Charge-orbital ordering and ferromagnetic chains in single-layered manganite crystals

T. Kimura,[1] K. Hatsuda,[1] Y. Ueno,[1] R. Kajimoto,[2] H. Mochizuki,[3] H. Yoshizawa,[3] T. Nagai,[4,5] Y. Matsui,[4] A. Yamazaki,[5] and Y. Tokura[1]

[1]*Department of Applied Physics, University of Tokyo, Tokyo 113-8656, Japan*

[2]*Department of Physics, Ochanomizu University, Tokyo 112-8610, Japan*

[3]*Neutron Scattering Laboratory, ISSP, University of Tokyo, Tokai, Ibaraki 319-1106, Japan*

[4]*Advanced Materials Laboratory, National Institute for Materials Science, Tsukuba, Ibaraki 305-0044, Japan*

[5]*Department of Resources and Environmental Engineering, Waseda University, Tokyo 169-8555, Japan*

(Received 22 October 2001; published 19 December 2001)

The temperature- and doping-induced variation of structural, magnetic, and transport properties has indicated unique switching of spin-charge-orbital states in the Mn-O sheets of single-layered manganite crystals, $Nd_{1-x}Sr_{1+x}MnO_4$. In the composition range of $0.75<x<0.9$, the magnetic ordering with alternate straight ferromagnetic chains occurs below $T_N \approx 150$ K in the orthorhombically distorted sheets which perhaps originate from the orbital ordering at 270 K. In the crystals with commensurate doping levels ($x=\frac{2}{3}$ and $\frac{3}{4}$), additional superlattice spots are observed with the propagation vectors $[\delta, \delta, 0]$ $[\delta \approx (1-x)/2]$, suggestive of the charge-orbital ordering with zig-zag ferromagnetic chains.

DOI: 10.1103/PhysRevB.65.020407 PACS number(s): 75.30.Vn, 61.14.−x, 75.25.+z

Charge, spin, and orbital ordering in transition-metal compounds with strongly correlated electrons have recently attracted significant research interest due to the possible relation to mechanisms of various phenomena such as metal-insulator transition, high-T_c superconductivity, colossal magnetoresistance, etc.[1] In particular, the compounds with the layered K_2NiF_4 structure and d^4 or d^9 electronic configuration can provide a unique arena to test important roles of the orbital correlations in the structural, electric, and magnetic properties, e.g., the orbital *antiferro* ordering induced ferromagnetism in K_2CuF_4 (Refs. 2 and 3) contrary to the antiferromagnetism in La_2CuO_4 with *ferro* orbital order. As another typical system, $La_{1-x}Sr_{1+x}MnO_4$ ($x=\frac{1}{2}$) with single-MnO_2 layers is the first compound in which the real-space ordering of the e_g orbitals has been confirmed by the resonant x-ray scattering technique.[4] However, the ordering structure in the single-layered manganites with $x \neq \frac{1}{2}$ have seldom been investigated in detail so far. In this communication, we report on the successive structural transitions relevant to the change of orbital state against variation of temperature and doping for single-layered manganite crystals, $Nd_{1-x}Sr_{1+x}MnO_4$ ($0.67 \leqslant x \leqslant 1.0$). By substituting La with Nd in the aforementioned $La_{1-x}Sr_{1+x}MnO_4$ system, we can prevent the chemical phase separation which takes place in the case of $La_{1-x}Sr_{1+x}MnO_4$,[5,6] and grow the single crystals over the whole concentration range. The switching of the orbital state of e_g-like electrons ($d_{3x^2-r^2}/d_{3y^2-r^2} \rightarrow d_{3x^2-r^2}$) is ascribed to the observed crossover from the charge-ordered antiferromagnetic state to the charge-disordered ferromagnetic chain state in the two-dimensional manganite crystal.

$Nd_{1-x}Sr_{1+x}MnO_4$ ($0.67 \leqslant x \leqslant 1.0$) crystals were grown by the floating zone method with use of a halogen-lamp image furnace at a rate of 6–12 mm/h in flowing air. We performed x-ray, electron, and neutron diffraction measurements on the grown crystals, which shows that all the crystals investigated here are of single phase and the $I4/mmm$ tetragonal structure at room temperature. Complete diffraction analyses indicate that the present $Nd_{1-x}Sr_{1+x}MnO_4$ system is free from such a chemical phase separation as observed in $La_{1-x}Sr_{1+x}MnO_4$ with $0.7<x<1.0$.[5,6] Resistivity of the crystals was measured by a standard dc four-probe method. Magnetization measurements were carried out with a commercial superconducting quantum interference device magnetometer.

We display in Fig. 1 the temperature profiles of the resistivity with current parallel (ρ_{ab}) and perpendicular (ρ_c) to

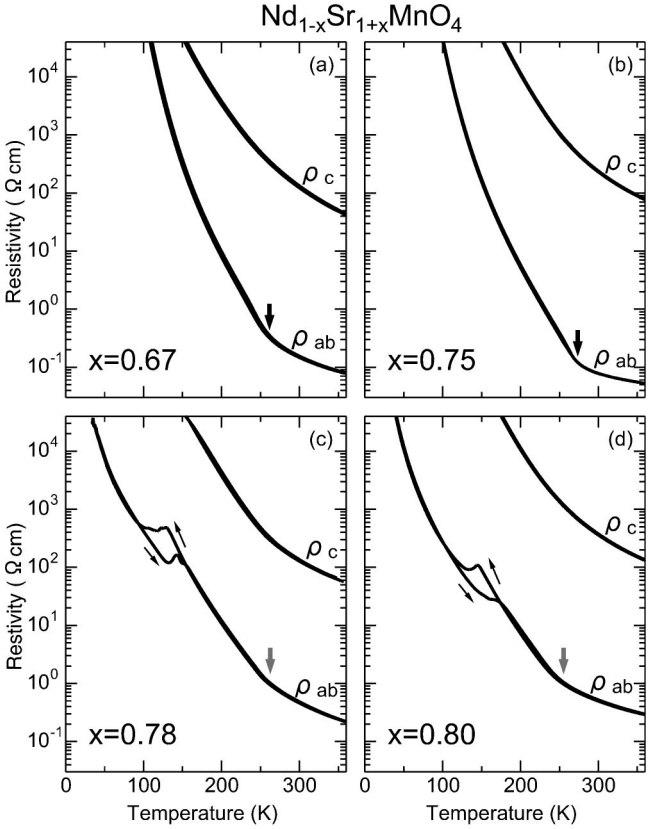

FIG. 1. Temperature dependence of resistivity with current parallel (ρ_{ab}) and perpendicular (ρ_c) to MnO_2 layers for $Nd_{1-x}Sr_{1+x}MnO_4$ ($0.67 \leqslant x \leqslant 0.80$) crystals.

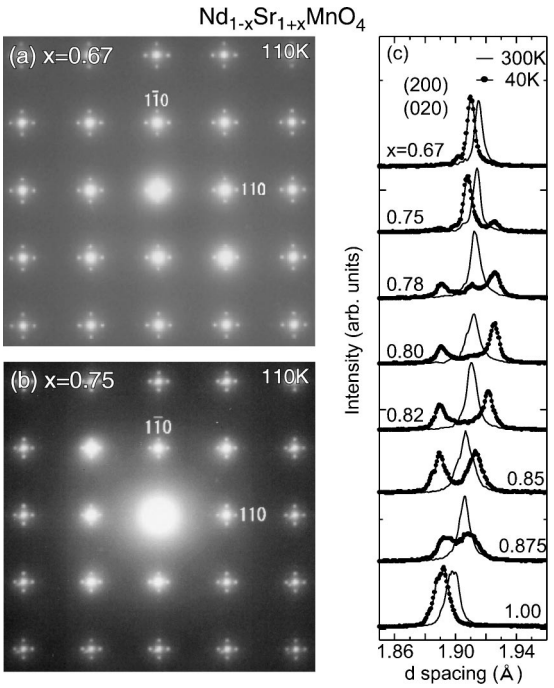

FIG. 2. [001] zone-axis electron diffraction patterns of (a) $x=0.67$ and (b) $x=0.75$ crystals at 110 K. The superlattice reflections with modulation wave vector $(\delta, \pm\delta, 0)$ ($\delta \approx \frac{1}{6}$ and $\frac{1}{8}$ for $x=0.67$ and $x=0.75$ crystals, respectively) are evident. (c) X-ray powder diffraction patterns around the (200) and (020) Bragg peaks in $Nd_{1-x}Sr_{1+x}MnO_4$ ($0.67 \leqslant x \leqslant 1.0$) at 300 K and 40 K.

the MnO_2 layers for selected crystals. For all the crystals, the anisotropy of resistivity (ρ_c/ρ_{ab}) is as large as 10^3 at room temperature. Although both ρ_{ab} and ρ_c show insulating temperature dependence over the whole composition range investigated here, several anomalies are observed in ρ_{ab}. A striking feature is that $x=0.67$ and 0.75 crystals exhibit a steep rise of ρ_{ab} toward lower temperatures at ~270 K (indicated by bold arrows in Fig. 1). With increasing x, the anomaly at ~270 K becomes dull, while another noteworthy feature emerges in the $x=0.78$ and 0.80 crystals. As seen in Figs. 1(c) and 1(d), the sudden drop of ρ_{ab} toward lower temperatures is evident at ~150 K. In addition, a considerable thermal hysteresis has been observed in the temperature region of $100\,\mathrm{K} \leqslant T \leqslant 150\,\mathrm{K}$.

To clarify the origin of the anomaly in ρ_{ab} at ~270 K for the $x=0.67$ and 0.75 crystals, measurements of electron diffraction patterns were performed with a high-voltage transmission electron microscope (Hitachi: H-1500). The diffraction pattern at room temperature can be indexed with the aforementioned $I4/mmm$ tetragonal unit cell. The most pronounced feature is the appearance of additional superstructure reflections at low temperatures. Upon cooling from room temperature the streaked spots appear along [110] and [1$\bar{1}$0] directions around the respective fundamental Bragg reflections at ~280 K. With further decreasing temperature, the streaked spots are transformed into well-ordered superlattice reflections below ~270 K. In Figs. 2(a) and 2(b), we show the [001] zone-axis electron diffraction patterns at 110 K for the $x=0.67$ and 0.75 crystals. The wave vector of these superlattice spots at 110 K can be described as $\vec{q}=\vec{a}^*[\delta,\delta,0]$ ($\vec{a}\cdot\vec{a}^*=2\pi$),[7] where δ is $\sim\frac{1}{6}$ and $\sim\frac{1}{8}$ for $x=0.67$ and 0.75 crystals, respectively. A similar variation of the wave vector with doping has been observed for a pseudocubic manganite, $La_{1-x}Ca_xMnO_3$ (Ref. 8) in which it is proposed that the e_g-like electrons localize and order along the diagonal direction of the Mn-O square lattice in the *ab* plane, forming the diagonal charge-orbital ordered stripes with a periodic spacing of $6\times d_{110}$ ($x=0.67$) or $8\times d_{110}$ ($x=0.75$). Considering these investigations of the superstructures and the anomaly in resistivity, the charge-orbital ordering may take place at ~270 K in the commensurate $x=0.67$ and $x=0.75$ crystal. Although we have not observed the similar additional superlattice reflections in higher x crystals, yet the small anomaly in ρ_{ab} for $x=0.78$ and 0.80 [indicated by gray arrows in Figs. 1(c) and 1(d)] signals the presence of short-range charge/orbital ordering.

Let us focus on the anomaly in resistivity at ~150 K observed for the $x=0.78$ and 0.80 crystals. To relate the resistive anomaly with the structural change, we have performed powder x-ray diffraction (XRD) measurements for $Nd_{1-x}Sr_{1+x}MnO_4$. Figure 2(c) displays the powder XRD patterns around the (200) and (020) Bragg peaks for samples with selected compositions at 300 K and 40 K. At 300 K least split between (200) and (020) Bragg peaks are observed for all of the specimens which have the $I4/mmm$ tetragonal structure. The remarkable composition dependence can be seen in the low-temperature patterns. For the specimens with $x=0.67$ and 1.0, the tetragonal structure appears to persist down to the lowest temperature. By contrast, in the intermediate composition range of $0.75 \leqslant x \leqslant 0.875$, a large split between (200) and (020) Bragg peaks can be observed at the low temperature (40 K). This implies that the orthorhombic phase with the lattice parameters $a \neq b$ appears at a temperature between 300 K and 40 K. The Rietveld analysis[9] indicates that the orthorhombic phase has the space group *Immm*. It is also to be noted that the both Bragg peaks related to the tetragonal and orthorhombic phases coexist in the composition range of $0.75 \leqslant x < 0.80$, and the fraction of the orthorhombic phase is increased with the increase of x. The split between (200) and (020) reflections is gradually suppressed with the further increase of $x(>0.8)$, and disappears at $x \geqslant 0.9$, which implies the suppression of the orthorhombicity and the reentrance to the tetragonal phase in $x \geqslant 0.9$.

To exemplify the tetragonal-to-orthorhombic phase transition in the specimens with $0.75 \leqslant x \leqslant 0.875$, we display in Fig. 3(a) the temperature profiles of the lattice parameters for the $x=0.78$ specimen, as determined from the Rietveld analysis of the powder XRD data. The measurements were performed in the warming run. The structural phase transition becomes evident from the significant change in the lattice parameters. For the $x=0.78$ specimen, the orthorhombic phase appears below $T_{OT} \approx 270\,\mathrm{K}$, and the phase separation between the orthorhombic and tetragonal phases takes place. All the data below T_{OT} have been refined with a two-phase model. The lattice parameters for the tetragonal phase monotonously decrease with decreasing temperature. Although the c axis for the orthorhombic phase and its temperature

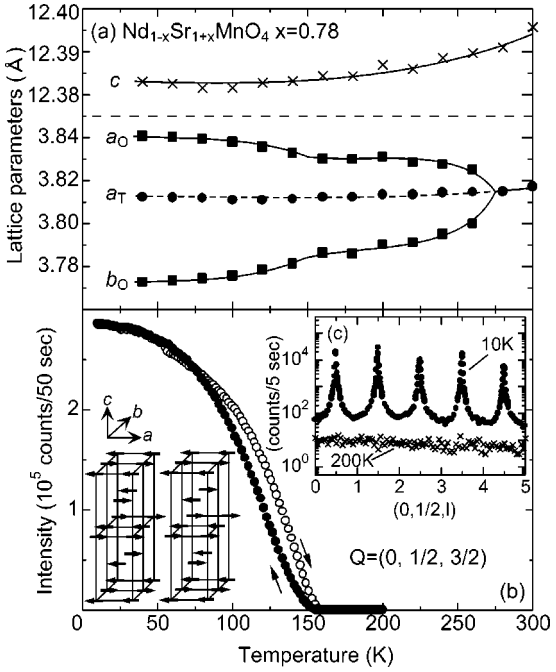

FIG. 3. (a) Lattice parameters as a function of temperature for $Nd_{1-x}Sr_{1+x}MnO_4$ ($x=0.78$) determined from powder x-ray diffraction. Closed and open circles are for the orthorhombic and tetragonal phases, respectively. Solid and dashed lines are merely guides to the eyes. (b) Temperature variation of the intensity of the $(0, \frac{1}{2}, \frac{3}{2})$ magnetic Bragg reflection from the $x=0.78$ single crystal measured by neutron diffraction. The closed and open circles represent the data measured in the cooling and warming runs, respectively. Inset: Schematic illustrations of the two types of antiferromagnetic structure in the *Immm* orthorhombic phase.

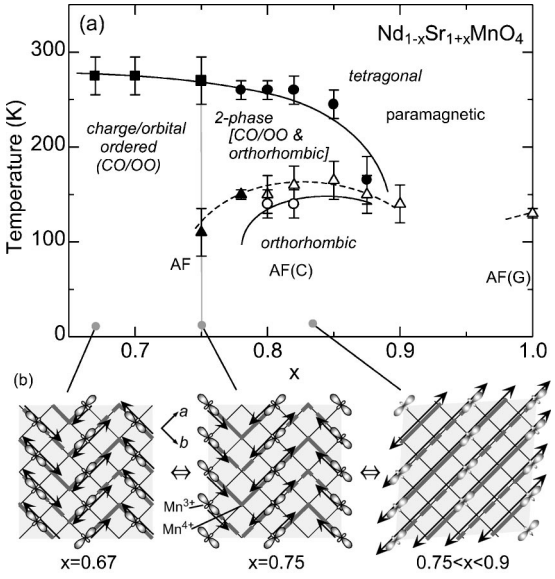

FIG. 4. (a) Electronic phase diagram of $Nd_{1-x}Sr_{1+x}MnO_4$ ($0.67 \leqslant x \leqslant 1.0$). Closed squares, closed circles, and open circles represent the charge-orbital ordering temperature T_{CO}, the onset temperature of the tetragonal-to-orthorhombic phase transition T_{OT}, and the onset temperature of single orthorhombic phase, respectively. Closed and open triangles represent the Néel temperature T_N determined from neutron diffraction and magnetization measurements, respectively. Solid and broken lines are the guide to the eyes for crystallographic and magnetic transitions, respectively. (b) Schematic illustration of a possible switching of the ferromagnetic chains between zigzag-type and straight-type which arise from the e_g-orbital ordering of alternate $d_{3x^2-r^2}/d_{3y^2-r^2}$ and coherent $d_{3x^2-r^2}$, respectively. Gray discontinuous lines represent possible magnetic chains with the same direction of the largest component of the spins (along [110] direction). (Gray solid lines are for the opposite direction.) Arrows indicate possible motion of e_g-like electrons.

dependence are identical with that for the tetragonal phase, the *b* axis rapidly decreases below T_{OT}, whereas the *a* axis increases. As a result, the orthorhombicity increases with decreasing temperature below T_{OT}.

The appearance of the *Immm* orthorhombic phase in the crystals with $0.75 \leqslant x \leqslant 0.875$ reminds us of the case of the bilayered manganites. In $La_{2-2x}Sr_{1+2x}Mn_2O_7$ ($0.74 < x < 0.92$), the magnetic ordering with the antiferromagnetically coupled ferromagnetic chains, so called *C*-type antiferromagnetic (AF) ordering,[10] takes place at a temperature below the tetragonal-to-orthorhombic phase transition temperature.[11] Considering the results of the bilayered manganite in which the ferromagnetic chains lie in MnO_2 bilayers, it can be expected that a similar chainlike magnetic structure within single MnO_2 layers exists in the present single-layered manganite. To determine the magnetic structure of the orthorhombic phase, neutron diffraction measurements on the $x=0.78$ crystal were performed with a triple axis spectrometer (4G-GPTAS) installed at the JRR-3M research reactor in JAERI, Tokai, Japan.

Figure 3(c) shows scans of the magnetic scattering along $\vec{q}=(0,\frac{1}{2},l)$ at 200 K and 10 K. Well-defined scatterings at half integer *l* are evident at 10 K, though not observed at 200 K, on the two-dimensional scattering background broadly distributed along *l*. The presence of $(0,\frac{1}{2},n+\frac{1}{2})$ peaks indicates that the magnetic unit cell has a dimension $a \times 2b \times 2c$ relative to the *Immm* cell, and that the magnetic structure within the *ab* (MnO_2) plane is the *C*-type antiferromagnetism with ferromagnetic chains along the long *a* axis, as illustrated in the insets of Fig. 3(b). The reflections at odd *n* and even *n* in Fig. 3(c) arise from the magnetic structures illustrated in the left and right insets, respectively, of Fig. 3(b). We display in Fig. 3(b) the intensity of a representative magnetic Bragg reflection $(0, \frac{1}{2}, \frac{3}{2})$ as a function of temperature. The temperature profile of the order parameter establishes the Néel temperature $T_N \approx 150$ K, and shows a thermal hysteresis below T_N in accord with that in resistivity [Fig. 1(c)]. As clearly seen in the temperature dependence of lattice parameters around T_N of Fig. 3(a), the magnetic ordering enhances the orthorhombicity of the lattice structure. In addition, the relative fraction of the orthorhombic phase steeply increases below T_N. The drop of ρ_{ab} at $T_N \approx 150$ K in the crystals with the *Immm* orthorhombic phase [Figs. 1(c) and 1(d)] may have intimate connection to the formation of the ferromagnetic chains along the *a*-axis. In the double-exchange model,[12] electrons can only hop between sites with ferromagnetically aligned core spins, and hence in the *C*-type AF phase the hopping is possible only along the ferromagnetic chains, rendering the conduction one-dimensional. Al-

though the present crystals have not been detwinned, we would observe more conducting behaviors along the ferromagnetic chains in twin-free crystals.

To sum up the current study, the crystallographic and magnetic phase diagram of $Nd_{1-x}Sr_{1+x}MnO_4$ is shown in Fig. 4(a). For understanding the phase diagram, we should take account of the orbital state of the e_g-like electrons of Mn^{3+}. Since a lattice form is strongly affected by the orbital character through the collective Jahn-Teller (JT) distortion, the observed structural change by varying temperature and doping level should reflect sensitively a change in the orbital state. The observed crystallographic superstructures in $x=0.67$ and $x=0.75$ crystals can be associated with the formation of the diagonal charge-orbital ordered stripes. The left and middle panels in Fig. 4(b) schematically display a possible Mn^{3+}-Mn^{4+} ordering and $d_{3x^2-r^2}/d_{3y^2-r^2}$ orbital-ordering on Mn^{3+} ions for $x=0.67$ and 0.75 crystals, respectively, which has been proposed for the pseudocubic manganite $La_{1-x}Ca_xMnO_3$ (so-called Wigner-crystal model)[13] and is also consistent with the observed ordering wave vector for the present single-layered manganite. In charge-orbital ordered $La_{1/3}Ca_{2/3}MnO_3$, there is striking discrepancy in the order pattern between the bistripe model[8] and the Wigner-crystal model.[13–15] According to the simulation study of the electron diffraction pattern,[16] the latter model much better describes the observed diffraction pattern with minimal intensities of higher harmonics of the superlattice spots for the present single-layered manganite. Further study of the crystallographic and magnetic structures for the present $Nd_{1-x}Sr_{1+x}MnO_4$ single crystals with a simple lattice form may provide significant information on this controversial issue.

Meanwhile, the appearance of the *Immm* orthorhombic phase in the composition range of $0.75<x<0.9$ can be understood in terms of stabilization of the $d_{3x^2-r^2}$ orbital state via the JT distortion. The schematic illustration for a possible orbital state is depicted in the right panel of Fig. 4(b). The $d_{3x^2-r^2}$-type orbitals are stabilized to maximize the transfer interaction of e_g-like electrons along the *a*-axis (*x* direction) and to give rise to the ferromagnetic (FM) double-exchange interaction only along the *a* axis. As a result, the *C*-type AF ordered state is realized in $Nd_{1-x}Sr_{1+x}MnO_4$ crystals, in which antiferromagnetically couple FM chains lie within single MnO_2 layers. The phase coexistence is seen in the vicinity of the phase boundary between the charge-ordered and charge-disordered *C*-type AF phases ($0.75\leqslant x\leqslant 0.78$). The ordering temperature of orbital ($T_{OO}\approx 270$ K) is higher than that for spin ($T_N\approx 150$ K), although the phase separation tendency for the orbital states is suppressed by the spin ordering. This implies that the orbital correlation is a driving force for the spin ordering but the spin ordering also affects the orbital state in the present layered manganite.

In conclusion, we have observed a doping-induced crossover from the charge-ordered state to the charge-disordered one-dimensional ferromagnetic [*C*-type antiferromagnetic (AF)] state in $Nd_{1-x}Sr_{1+x}MnO_4$ crystals. There are a great number of studies that deal with the competition or coexistence between the ferromagnetic (FM) and the charge-orbital ordered *CE*-type AF phases in magnetoresistive manganites.[17] However, only a few theoretical studies have been reported on those between the charge-orbital ordered *CE*-type and the *C*-type AF states.[18,19] Most of them focus on the similarity between the zigzag FM stripe in the *CE*-type AF state and the straight FM stripe in the *C*-type one. In both cases, the e_g electrons can hop along these FM chains. The presently observed variation of the crystallographic and magnetic structures against the doping-level can be viewed as a switching between the charge-orbital ordered C_xE_{1-x}-type (zigzag FM stripe)[20] and the *C*-type (straight FM stripe) AF states in spin sector, and a switching between the *antiferro* $d_{3x^2-r^2}/d_{3y^2-r^2}$ and the *ferro* $d_{3x^2-r^2}$ orbital-ordered states.

We thank S. Ishihara for helpful discussions. This work was supported in part by NEDO and Grant-In-Aids for Scientific Research from MEXT, Japan.

[1] M. Imada, A. Fujimori, and Y. Tokura, Rev. Mod. Phys. **70**, 1039 (2000).
[2] D. I. Khomskii and K. I. Kugel, Solid State Commun. **13**, 763 (1973).
[3] Y. Ito and J. Akimitsu, J. Phys. Soc. Jpn. **40**, 1333 (1976).
[4] Y. Murakami, H. Kawada, H. Kawata, M. Tanaka, T. Arima, Y. Moritomo, and Y. Tokura, Phys. Rev. Lett. **80**, 1932 (1998).
[5] Y. Moritomo, Y. Tomioka, A. Asamitsu, Y. Tokura, and Y. Matsui, Phys. Rev. B **51**, 3297 (1995).
[6] Wei. Bao, C. H. Chen, S. A. Carter, and S.-W. Cheong, Solid State Commun. **98**, 55 (1996).
[7] The observed two different modulations along the [110] and $[1\bar{1}0]$ can originate from twin domains rotated by 90° to each other.
[8] S. Mori, C. H. Chen, and S-W. Cheong, Nature (London) **392**, 473 (1998).
[9] F. Izumi, *Rietveld Method*, edited by R. A. Young (Oxford University Press, Oxford, 1993), Chap. 13.
[10] E. O. Wollan and W. C. Koehler, Phys. Rev. **100**, 545 (1955).
[11] C. D. Ling, J. E. Millburn, J. F. Mitchell, D. N. Argyriou, J. Linton, and H. N. Bordallo, Phys. Rev. B **62**, 15 096 (2000).
[12] C. Zener, Phys. Rev. **82**, 403 (1951).
[13] P. G. Radaelli, D. E. Cox, L. Capogna, S.-W. Cheong, and M. Marezio, Phys. Rev. B **59**, 14 440 (1999).
[14] M. T. Fernandez-Diaz, J. L. Martinez, J. M. Alonso, and E. Herrero, Phys. Rev. B **59**, 1277 (1999).
[15] R. Wang, J. Gui, Y. Zhu, and A. R. Moodenbaugh, Phys. Rev. B **61**, 11 946 (2000).
[16] T. Nagai and Y. Matsui (unpublished).
[17] A. Moreo, S. Yunoki, and E. Dagotto, Science **283**, 2034 (1999), and references therein.
[18] J. van den Brink, G. Khaliullin, and D. Khomskii, Phys. Rev. Lett. **83**, 5118 (1999).
[19] T. Hotta, Y. Takada, H. Koizumi, and E. Dagotto, Phys. Rev. Lett. **84**, 2477 (2000); T. Hotta, A. L. Malvezzi, and E. Dagotto, Phys. Rev. B **62**, 9432 (2000).
[20] E. Dagotto, T. Hotta, and A. Moreo, Phys. Rep. **344**, 1 (2001).